

Ordinal Synchronization: Using ordinal patterns to capture interdependencies between time series

I. Echegoyen^{a,b,*}, V. Vera-Ávila^c, R. Sevilla-Escoboza^c, J.H. Martínez^{d,b},
J.M. Buldú^{a,b}

^aLaboratory of Biological Networks, Centre for Biomedical Technology. Universidad Politécnica de Madrid, Spain

^bComplex Systems Group & G.I.S.C., Universidad Rey Juan Carlos, Móstoles, Spain

^cCentro Universitario de Los Lagos, Universidad de Guadalajara, Lagos de Moreno, Mexico

^dINSERM-UM1127, Sorbonne Université, ICM-Hôpital Pitié Salpêtrière, Paris, France

Abstract

We introduce Ordinal Synchronization (OS) as a new measure to quantify synchronization between dynamical systems. OS is calculated from the extraction of the ordinal patterns related to two time series, their transformation into D -dimensional ordinal vectors and the adequate quantification of their alignment. OS provides a fast and robust-to noise tool to assess synchronization without any implicit assumption about the distribution of data sets nor their dynamical properties, capturing in-phase and anti-phase synchronization. Furthermore, varying the length of the ordinal vectors required to compute OS it is possible to detect synchronization at different time scales. We test the performance of OS with data sets coming from unidirectionally coupled electronic Lorenz oscillators and brain imaging datasets obtained from magnetoencephalographic recordings, comparing the performance of OS with other classical metrics that quantify synchronization between dynamical systems.

*I. Echegoyen would like to thank the Foundation Tatiana Pérez de Guzmán el Bueno for financially supporting this research. R.S.E. acknowledges support from Consejo Nacional de Ciencia y Tecnología call SEP-CONACYT/CB-2016-01, grant number 285909. J.M.B. is supported by Spanish Ministry of Economy and Competitiveness under Projects FIS2013-41057-P and FIS2017-84151-P. J.H.M. acknowledges M. Chavez for his valuable comments.

*Corresponding author. *E-mail address: nacho.e.blanco@gmail.com*

Keywords: Synchronization, ordinal patterns, in-phase synchronization, anti-phase synchronization, nonlinear electronic circuits, brain imaging data sets.

Since the seminal work of Huygens about the coordinated motion of two pendulum clocks (referred to as “an odd kind of sympathy”) [1], the study of synchronization in real systems has been one of the major research lines in nonlinear dynamics. From fireflies to neurons, synchronization has been reported in a diversity of social (e.g., human movement or clapping) [2, 3], biological (e.g., brain regions or cardiac tissue) [4, 5] and technological systems (e.g., wireless communications or power grids) [6, 7], being in many cases a fundamental process for the functioning of the underlying system. However, despite being an ubiquitous phenomenon, the detection and quantification of synchronization can be a difficult task. The main reasons are the diversity of kinds of synchronization [8], the complexity of interaction between dynamical systems [9], the existence of unavoidable external perturbations [10] or the inability of observing all variables of a real system [11], just to name a few.

As a consequence, there is not a unique way of quantifying the amount of synchronization in real time series and a series of metrics have been proposed with this purpose. As a rough approximation, these metrics can be classified into three main groups: (i) linear, (ii) nonlinear and (iii) spectral metrics. While linear metrics, such as the Pearson correlation coefficient, are the most straightforward to be calculated and less time consuming, they suppose the existence of a linear correlation between time series, an assumption that is not fulfilled in the majority of real cases. On the other hand, nonlinear metrics assume a certain nonlinear coupling function f_n between a variable X and a variable Y , such as $X = f_n(Y)$. However the estimation of the nonlinear function renders impossible in the majority of cases and certain assumptions have to be assumed for quantifying synchronization. Measures such as the mutual information or the phase locking value are examples of nonlinear metrics, the former assuming a certain statistical interdependency between signals and the latter considering only a phase relation. Finally, spectral metrics, such as the coherence or the imaginary part of coherence, translate the problem to the spectral domain, analyzing the relation between the spectra obtained from the original time series assuming linear/nonlinear relations (see [12] for a thorough review about metrics quantifying synchronization in real data sets).

In the current paper we are concerned about using ordinal patterns, a

symbolic representation of temporal data sets, to define a new metric that is able to reveal the synchronization between time series. Bahraminasab *et. al.* [13] used a symbolic dynamics approach to design a directionality index parameter. Transforming the increment between successive points within a times series into ordinal patterns, authors calculated the mutual information between a process X_1 at time t and a process X_2 at time $t + \tau$ and next obtained the directionality index as defined in [14]. Applying this methodology to respiratory and cardiac recordings it is possible to quantify how respiratory oscillations have more influence on cardiac dynamics than vice-versa [13]. More recently, Li *et al.* used a similar indicator to evaluate the directionality of the coupling in time series consisting of spikes [15]. Using the Izhikevich neuron model [16], authors showed how that methodology was robust for weak coupling strengths, in the presence of noise or even with multiple pathways of coupling between neurons. More recently, Rosário *et. al.* [17] used the ordinal patterns observed in EEG datasets, also known as “motifs” [18], to construct time varying networks and analysed their evolution along time and the properties of the averaged functional network. Specifically, the amount of synchronization between a pair of recorded electrodes of an EEG was obtained by evaluating the number of ordinal patterns co-occurring at the same time but also at a given lag $\lambda = 1$ time steps. Using both positive and negative values of λ authors were able to quantify the direction of the interaction between the two time series, i.e., the causality, to further construct temporal time networks. Next, they showed how the resulting time varying functional networks were able to identify those brain regions related to information processing and found differences between healthy individuals and patients suffering from chronic pain [17].

In this paper, we also propose the use of symbolic dynamics to evaluate the level of synchronization between time series. However, our methodology consists in a measure of synchronization that does not take into account the existence of a delay time between time series, despite further adaptation to this case is also possible (see Section Conclusions). As in the case of [13, 18, 17], we take advantage of the transformation of a time series into a concatenated series of D -dimensional ordinal patterns [19] that allow us to quantify the amount of synchronization between two (or more) symbols sequences. The main advantage of our methodology is that it takes into account both the in-phase and anti-phase synchronization of two dynamical systems, the latter being disregarded in the aforementioned proposals based on ordinal patterns.

We have calculated the *OS* of two kind of data sets: (i) unidirectionally coupled Lorenz electronic systems and (ii) magnetoencephalographic (MEG) recordings measuring the activity of 241 sensors placed at the scalp of an individual during resting state. Next, we compared the amount of synchronization computed by *OS* with respect to those obtained from classical metrics like *phase locking value* (PLV), *mutual information* (MI), *spectral coherence* (SC) and *Pearson correlation* (r).

1. Materials and Methods

1.1. Defining Ordinal Synchronization

To compute the (OS) between two time series X and Y , we first extract their D -dimensional ordinal patterns [19]. In this way, we choose a length D and divide both time series of length M into $L = M/D$ equal segments. Next, we obtain the order of the values included inside each segment, also called the *ordinal patterns*: 1

$$X_t = \{x_1, x_2, \dots, x_D\} \mapsto V_t = \{v_1, v_2, \dots, v_D\} \quad (1)$$

$$Y_t = \{y_1, y_2, \dots, y_D\} \mapsto W_t = \{w_1, w_2, \dots, w_D\} \quad (2)$$

where V_t and W_t are the *ordinal vectors* inside the segment given by $\{t, t + 1, \dots, t + D - 1\}$, elements refer to the ordinal position of the values in X_t and Y_t , respectively. Note that the elements in V_t and W_t are natural numbers ranging from 0 to $D - 1$. The higher the value in the time series, the higher the corresponding element in the ordinal vector. Following the example depicted in Fig. 1, where $D = 4$, we obtain:

$$X_t = \{-1.22, 0.44, 0.91, 0.63\} \mapsto V_t = \{0, 1, 3, 2\} \quad (3)$$

$$Y_t = \{1.34, 0.12, 0.78, 0.57\} \mapsto W_t = \{3, 0, 2, 1\} \quad (4)$$

Then, we take the euclidean norm of each ordinal vector.

$$\|V_t\| = \sqrt{v_1^2 + v_2^2 + \dots + v_D^2} = \sqrt{0^2 + 1^2 + \dots + (D - 1)^2} \quad (5)$$

and we call $V_t^N = V_t/\|V_t\|$ and $W_t^N = W_t/\|W_t\|$ the normalized vectors. Note that this step only depends on the length D .

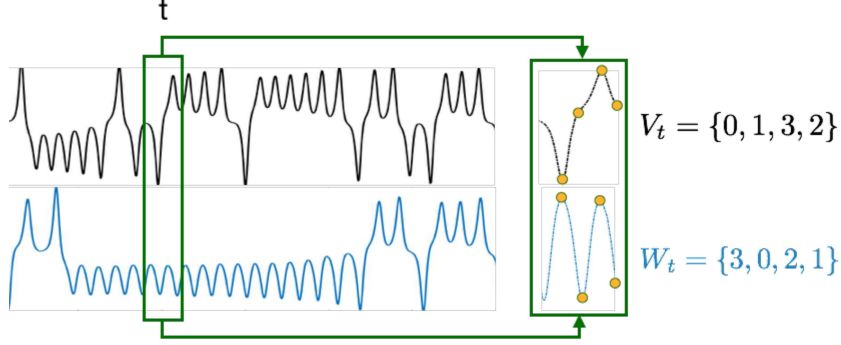


Figure 1: Qualitative example of ordinal vectors extraction from two time series. Here $D = 4$ is the length of the ordinal patterns. From each time series, an ordinal vector containing the desired number of samples is obtained by ranking its D values at time t , inside the vector.

Now, we define the raw value of the *instantaneous ordinal synchronization* at time t (IOS_t^{raw}) as the dot product between both ordinal vectors $IOS_t^{raw} = \sum_{i=1}^D v_{i,t} w_{i,t}$ (i.e., $V_t^N \cdot W_t^N$). For a more intuitive interpretation, we linearly rescale the value of IOS_t^{raw} to be bounded between -1 and 1 :

$$IOS_t = 2 \left(\frac{IOS_t^{raw} - \min}{1 - \min} - 0.5 \right) \quad (6)$$

where \min is the minimum possible value of the scalar product between two ordinal vectors. Note that, since the elements of the ordinal vectors are always positive and have only one component equal to zero, the lowest possible scalar product between V_t and W_t is obtained when the order of the elements of vector V_t is inverted in W_t . In our example:

$$\min = \frac{0(4) + 1(3) + 2(2) + 3(1) + 4(0)}{0^2 + 1^2 + 2^2 + 3^2 + 4^2} \quad (7)$$

In general, for any vector of length D :

$$\min = \frac{0(D-1) + 1(D-2) + \dots + (D-2)1 + (D-1)0}{0^2 + 1^2 + \dots + (D-1)^2} \quad (8)$$

Following the normalization in 6), we ensure that two ordinal vectors that follow opposite evolutions will unambiguously lead to a value of $IOS_t = -1$, and two vectors whose elements have the same order will have an $IOS_t = 1$. Being $L = M/D$ the total number of ordinal vectors in time series of M points, the final value of the ordinal synchronization $OS\{X, Y\}$ for a given pair of time series X and Y is obtained averaging the instantaneous values

of IOS_t along the whole time series:

$$OS\{X, Y\} = \langle IOS_t \rangle \quad (9)$$

Since we consider the IOS_t of consecutive (i.e., non-overlapping) time windows, the value of t in Eq. 9 is given by the expression $t = 1 + iD$, with i being a natural number bounded by $0 \leq i \leq L - 1$. Note that it is also possible to define a *sliding OS* just by increasing t in one unit for every IOS_t instead of considering consecutive windows.

1.2. Experimental results: Electronic Lorenz Systems

We analyzed the transition to the synchronized regime of two coupled Lorenz oscillators [20]. We implemented an electronic version of the Lorenz system, whose equations are detailed in Appendix B. Two Lorenz circuits are coupled unidirectionally in a master-slave configuration (see Fig. 2) with a coupling strength κ that can be modified. Our experiments include two conditions: in the first one, κ is modified in the absence of external noise; in the second one, κ varies in presence of Gaussian noise with band selection. The (AI0-AI3) input ports of a data acquisition (DAQ) card are used for sampling the x and z variables of each circuit, while the output ports AO0 and AO1 generate two different noise signals (ξ_1, ξ_2) that perturb the dynamics of the Lorenz circuits through variable x of each circuit. In this way, an external source of noise can be introduced to check the robustness of the experiments. The circuit responsible of the coupling strength κ is controlled by a digital potentiometer XDCP, which is adjusted by digital pulses from ports P00 and P01. Noisy signals were designed in LabVIEW, using a Gaussian White Noise library [21] that generates two different Gaussian-distributed pseudorandom sequences bounded between $[-1 \ 1]$. All the experimental process is controlled by a virtual interface in LabVIEW 2016 (PC).

The experiment works in the following way: First, κ is set to zero and digital pulses (P00 and P01) are sent to the digital potentiometer until the highest value of κ is reached. Second, variables x and z of the circuits are acquired by the analog ports (AI0-AI3) in order to compute the synchronization metrics. Initially, we have obtained all results for $\xi_1 = \xi_2 = 0$, i.e., in the absence of external noise, and then, after a moderate amount of noise is introduced, all synchronization metrics are calculated again (See Appendix C). Every signal, with or without noise, has a length of 30000 samples.

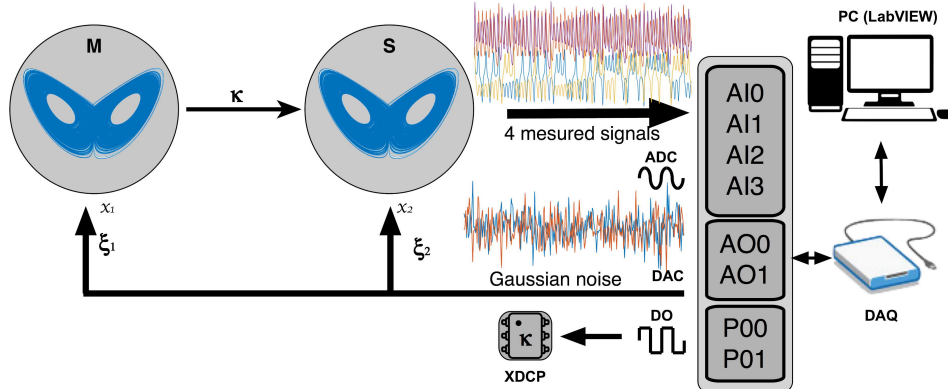


Figure 2: Schematic representation of Lorenz systems in a master-slave configuration. Signals are measured through a DAQ card (Ports AI0-AI3) and stored in a PC. Digital output (P00-P01) ports and XDCP control the value of coupling strength κ . Analog output ports (AO0-AO1) introduce the external noise signals ξ_1 and ξ_2 perturbing the x_1 master (M) and x_2 slave (S) variables, respectively.

1.3. Applications to magnetoencephalographic recordings

We have checked the performance of the *OS* in the context of neuroscientific datasets. Specifically, we quantified the level of synchronization between pairs of channels of MEG recordings. Data sets have been obtained from the Human Connectome Project (for details, see [22] and <https://www.humanconnectome.org>). The experimental data sets consist of 30 MEG recordings of an individual during resting state for a period of approximately 2 minutes each. During the scan, the subject were supine and maintained fixation on a projected red crosshair on a dark background. Brain activity was scanned with 241 magnetometers on a whole head MAGNES 3600 (4D Neuroimaging, San Diego, CA, USA) system housed in a magnetically shielded room. The root-mean-squared noise of the magnetometers is about 5 fT/sqrt(Hz) on average in the white-noise range (above 2 Hz). Data was recorded at sampling rate of $f_s \approx 508.63 Hz$. Five current coils attached to the subject, in combination with structural-imaging data and head-surface tracings, were used to localize the brain in geometric relation to the magnetometers and to monitor and partially correct for head movement during the MEG acquisition. Artifacts, bad channels, and bad segments were identified and removed from the MEG recordings, which were processed with

a pipeline based on independent component analysis to identify and clean environmental and subject’s artifacts [22].

2. Results

2.1. Nonlinear electronic circuits

In order to assess the validity of OS , we have explored its performance for different values of D , from 3 to the full length of the time series under evaluation. Since it is the first time OS is used, we have compared it to classical measures of correlation, namely Pearson correlation coefficient (r), spectral coherence (SC), phase locking value (PLV) and mutual information (MI). We have used two kinds of data sets to validate OS , on the one hand, experimental time series from nonlinear electronic circuits, and on the other hand, MEG recordings.

First, we take advantage of the ability of controlling the coupling strength between electronic circuits and investigate how OS changes as two dynamical systems smoothly vary their level of synchronization from being unsynchronized to completely synchronized. Specifically, two electronic Lorenz systems are unidirectionally coupled with a parameter κ controlling their coupling strength (see Appendix B for details). Initially, we do not perturb the oscillators with external noise (see Appendix C for the case of including external noisy signals). However, we can not avoid the intrinsic noise of the electronic circuits together with the tolerance of the electronic components (between 5 % and 10 %). Figure 3 shows how the value of OS changes as the coupling strength κ is increased from zero. Since the value of OS depends on the length of the ordinal vectors, we show the results for three different values: $D = 3$ (Fig. 3A), $D = 500$ (Fig. 3B) and $D = 1000$ (Fig. 3C). Note that, by increasing the length of the vectors, we are obtaining the amount of synchronization at different time scales. Together with OS , we plot the values of the rest of synchronization metrics in (A), (B) and (C), which remain unaltered in the three plots (since they do not depend on D).

In all cases, we observe that OS increases for low to moderate values of κ and remains at a high value once a certain threshold is reached. This behaviour is similar to the rest of the synchronization metrics. However, both MI and SC seem to saturate at values of κ higher than r , PLV and OS , which seem to reach a plateau around $\kappa = 40$. Figure 3D shows the comparison of OS for the three different values of D . Here, we can also observe how at $D = 3$, OS has a different qualitative behaviour from $D = 500$

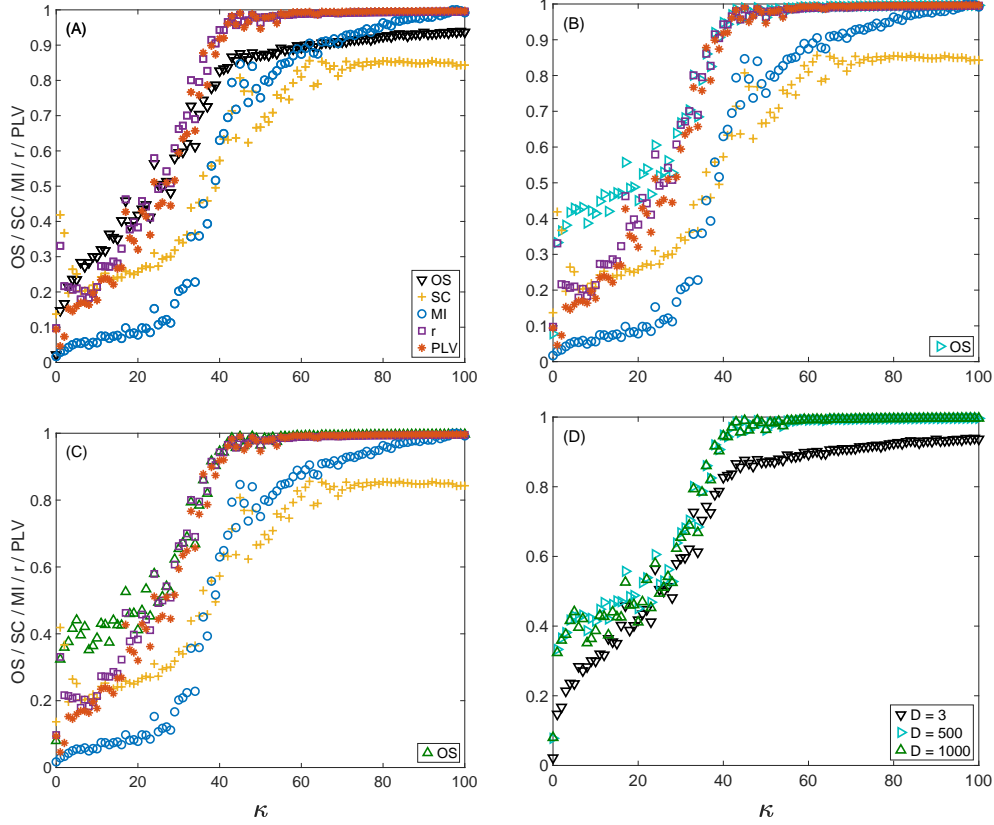


Figure 3: Synchronization against coupling strength κ as measured with *PLV* (red stars), *SC* (yellow crosses), *MI* (light blue circles), *r* (purple squares). *OS* (triangles) is plotted for $D = 3$ (A) (black downward-pointing), $D = 500$ (B) (turquoise right-pointing) and $D = 1000$ (C) (green upward-pointing). For comparison purposes, plot (D) shows *OS* against κ for different vector lengths, $D = 3$, $D = 500$ and $D = 1000$.

and $D = 1000$, since it stays around 0.9 and does not reach 1 as in the windows of longer lengths. The reason is the existence of intrinsic noise of the electronic circuits, that affects much more the alignment of the ordinal vectors of shorter lengths than those with higher dimensions.

Figure 4 shows the average correlation (ρ) between each D -dependent *OS* and the rest of synchronization metrics with zero noise. Note that correlations are higher than 0.92 in all cases, although it seems to be certain vector lengths that maximize these correlations. Also note that correlations with *PLV* and *r* are the highest and, in all cases, very close to 1. At the same

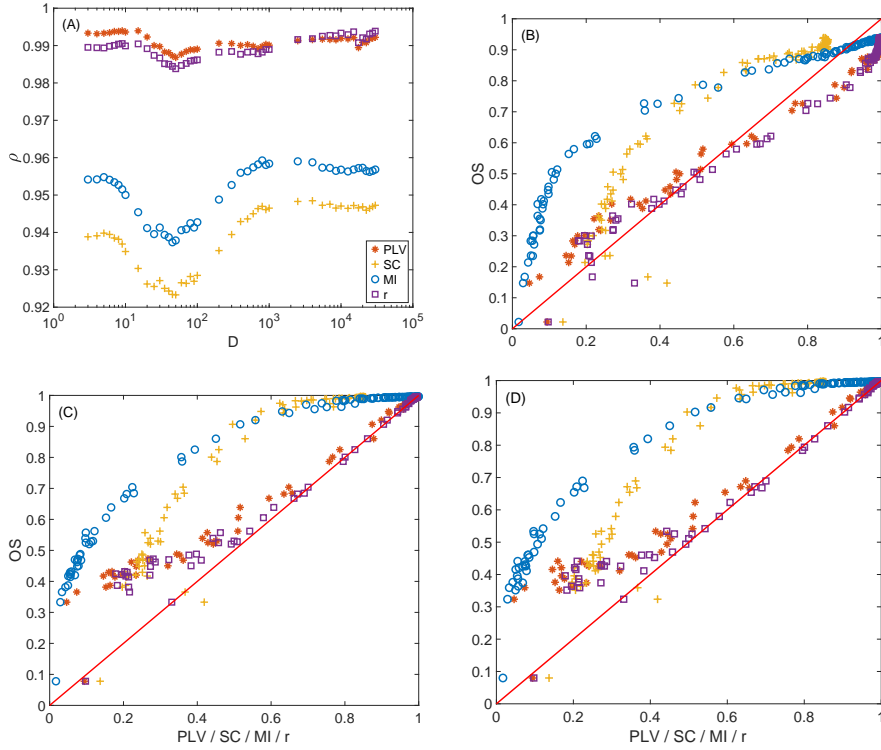


Figure 4: Panel (A) shows the average correlation (ρ) between each synchronization measure and OS depending on the vector length D . Panels (B)-(D) show the correlation between OS and all other synchronization measures varying the coupling strength (from 0 to 100), for $D = 3$ (B), $D = 500$ (C) and $D = 1000$ (D). Following the same notation as in Fig. 3, synchronization measures are (MI ; blue), (r ; purple), (SC ; yellow) and (PLV ; red). The red line corresponds to $y = x$.

time, MI and SC show lower correlations that, in turn, seem to be more dependent on the value of the vector length D (see Fig. 4A).

We can investigate how OS is related to the rest of the synchronization metrics in more detail by setting the length of the ordinal vectors to a given value (3, 500 or 1000 in this case) and observe the influence of the level of synchronization (Fig. 4B, C and D). For any of the three selected lengths, OS shows a linear relation with PLV and r , especially at values of OS higher than 0.5. However, the relation with SC and MI seems to be nonlinear in all cases. Interestingly, for low levels of synchronization, OS increases much faster than these two latter metrics. While SC saturates around 0.8,

MI finally increases faster than OS only for high values of synchronization, eventually reaching the value of OS around 1. Also note how, in the case of $D = 3$ (Fig. 4B), the intrinsic noise of the electronic circuits prevents OS to reach the value of one. This behaviour can be observed even clearer in the case of adding more noise into the system, as shown in Appendix C.

2.2. MEG signals

The second application is the evaluation of the level of synchronization between the 241 sensors measuring the activity of an individual during resting state. Concretely, we have 30 recordings of 2 minutes each. In this case, we can not control the amount of coupling between sensors but, alternatively, we have a diversity of levels of synchronizations between all possible pairs of sensors. Figure 5 shows how the correlations between OS and the rest of the metrics change depending on D . As we can observe, correlations are high in all cases except for SC , but this one saturates around the same D as the other synchronizations does.

As in the case of the electronic Lorenz oscillators, tuning the value of D allows to obtain values of OS closer, or more correlated, to other metrics. In fact, two different regions are clearly observed: (i) for values of $D \leq 20$ the correlation of OS with PLV, r , and MI increases with D , while (ii) for $D > 20$ correlation saturates around the highest value, being r the metric with the highest correlation. Interestingly, the behaviour of the SC goes in the opposite direction, decreasing for higher values of D .

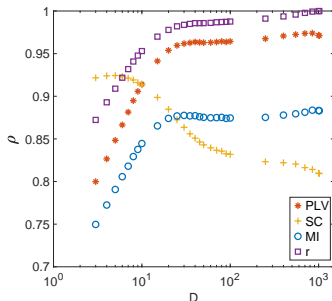


Figure 5: Correlation ρ between different synchronization metrics and OS as a function of the length D of the ordinal vectors. As in previous figures: PLV (red), SC (yellow), MI (blue), r (purple).

In order to gain insights about how the behaviour of OS depends on the level of synchronization and the length D , we plot three different cases in

Figure 6. In (A), we show the time series of two highly-correlated sensors, with their corresponding OS value depending on D (Fig. 6D). Plot (B) and (C) show the cases of two uncorrelated and negatively correlated sensors, respectively, with their values of OS (Fig. 6E and F). Note that for the positive (negative) case, correlations tend to stabilize as D grows, indicating the existence of a certain temporal scale at which synchronization is increased (reduced). Also note that, when time series are not correlated, this pattern is not that clear, and OS values remain low for any value of D .

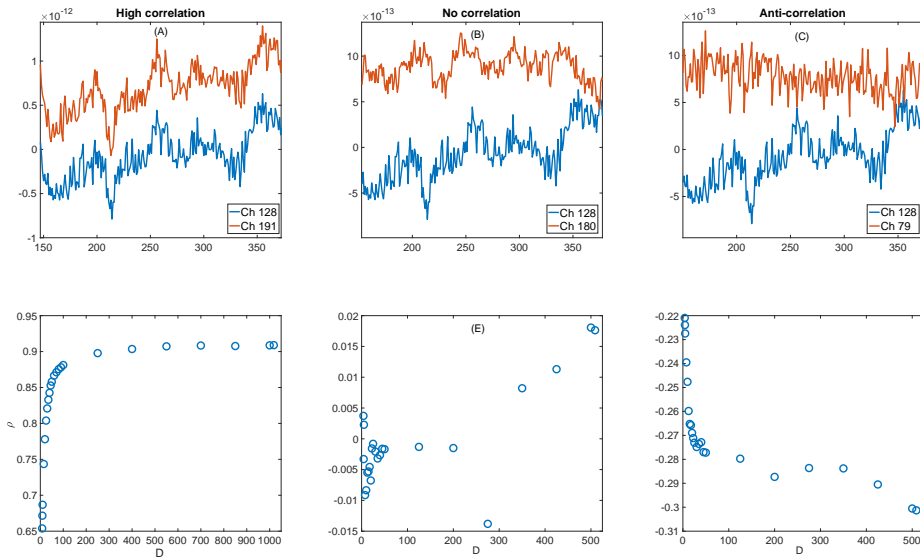


Figure 6: Example of the MEG time series and their corresponding OS vs D for three different situations: two sensors with high correlation (A and D), no correlation (B and E) and anti-correlated (C and F). Upper panel shows part of the raw signals recorded at the sensors while bottom panel shows OS depending on the length D .

We had analyzed the relation of OS with the rest of the metrics according to the level of synchronization. Figure 7 shows a panel of plots capturing the correlations between OS and all other synchronization metrics for the MEG signals. Left plots show the case of $D = 3$, middle plots show $D = 500$ and right plots show $D = 1000$. Different conclusions can be drawn depending on the synchronization metric OS is compared to. In the case of MI (first row), the existence of a nonlinear correlation between both metrics arises. However, this correlation decreases with the length of the ordinal vectors, becoming rather noisy for $D = 3$. This behaviour is induced by the intrinsic

noise of the MEG signals that, as in the case of electronic circuits, affects the value of OS when short lengths of the ordinal vectors are considered. Also note that MI is not able to distinguish positive from negative correlations between time series, a fact that makes OS an interesting metric when both kind of synchronizations are expected. In our case, for example, despite the highest values of OS are close to 1, the lowest ones arrive to -0.35 , indicating the existence of anti-correlated dynamics between certain pairs of sensors. A similar behaviour is reported in the case of the comparison with PLV (second row). Again, a nonlinear relation exists between both metrics, which is rather noisy at low values of the ordinal vector lengths ($D = 3$). PLV has also the same limitations as MI , since it does not differentiate between positive and negative correlations. Interestingly, the relation with SC is different from the two previous metrics (third row). Despite a nonlinear correlation between OS and SC seems to be present in the plots, this correlation is deteriorated with the increase of D .

Finally, OS shows a clear linear correlation with r (bottom row), which, as in the case of MI and PLV becomes noisy for low values of D . Note that, the loss of correlation for low values of D is indicating that, at short time scales, OS is capturing a different pattern of synchronization than at large scales. This is an interesting feature of OS which suggests that, when using it as a metric to evaluate synchronization between signals, it is appealing to carry out an analysis depending on the vector length in order to reveal the existence of different levels of synchronization at different time scales.

3. Conclusions

We have introduced the *Ordinal Synchronization* (OS), a new metric to evaluate the level of synchronization between time series by means of a projection into ordinal patterns. We have checked the performance of OS with two kinds of experimental data sets obtained from: (i) unidirectionally coupled nonlinear electronic circuits and (ii) 30 magnetoencephalographic recordings containing the signals of 241 channels. There are several advantages of using OS . First, it is able to capture in-phase and anti-phase synchronization. Second, tuning the length of the ordinal vectors D , it is possible to evaluate the level of synchronization at different time scales. Third, it is not necessary to assume any *a priori* property of the time series, such as stationarity or linear coupling. Fourth, the calculation of OS is extremely fast, especially when compared with other metrics such as MI . On the other hand, we have

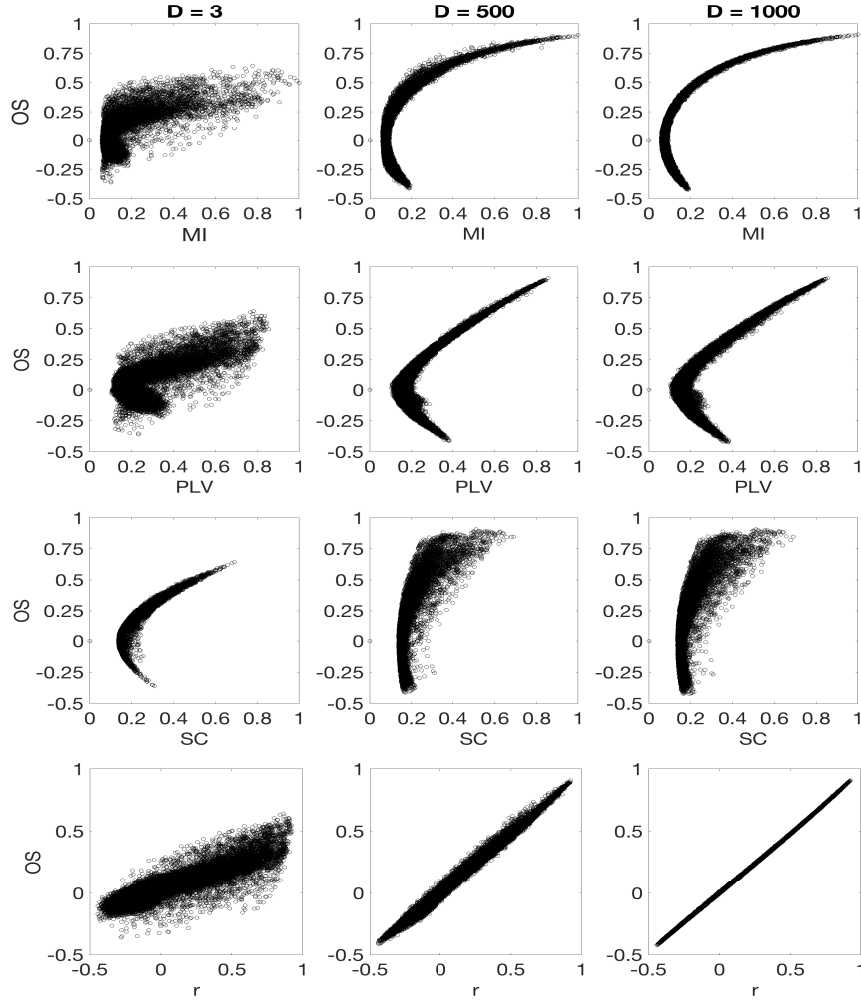


Figure 7: Correlation between OS and other synchronization metrics in MEG data sets: MI (upper row), PLV (second row), SC (third row) and r (bottom row). Each column corresponds to an OS obtained with different lengths D of the ordinal vectors: $D = 3$ (left column), $D = 500$ (middle column) and $D = 1000$ (right column).

also seen that one of the elements affecting the value of OS is the existence of noise, which reduces its value if the dimension of the ordinal vectors is low. However, depending on the application, this fact can also be considered as an indicator of the existence of noise.

A comparison with other classical metrics to evaluate synchronization has been carried out showing some similarities and differences. In general, OS shows high correlation with r and PLV , something that can be explained by the way OS is constructed. Ordinal patterns filter part of the information

contained in the amplitude of the signal, maintaining just the ranking in the time series. This is something between considering just the phase (*PLV*) or just the amplitude (*r*), since differences in amplitude are not related to changes in the *OS* parameter as long as the ranking is not modified.

In view of all, we believe that the use of *OS* can be interesting (but not restricted to) for evaluating the amount of synchronization in neuroscientific data sets, where in-phase and anti-phase synchronization are known to co-exist, together with coordinations at different time scales.

Appendix A: Coordination metrics

A.1. Pearson's Correlation Coefficient

The Pearson's correlation coefficient *r* consists of a covariance scaled by variances, thus capturing linear relationships among variables. From the equations of the variance (of *X* and *Y*) and covariance (of *XY*), we obtain Pearson Correlation Coefficient as:

$$S_Y = \sqrt{\frac{\sum (Y_i - \bar{Y})^2}{n - 1}} = \sqrt{\frac{\sum y_i^2}{n - 1}} \quad (10)$$

$$S_X = \sqrt{\frac{\sum (X_i - \bar{X})^2}{n - 1}} = \sqrt{\frac{\sum x_i^2}{n - 1}} \quad (11)$$

$$S_{XY} = E[(X - E[X])(Y - E[Y])] \quad (12)$$

$$r = \frac{S_{XY}}{S_X S_Y} \quad (13)$$

Pearson's correlation is a measure of linear dependence between any pair of variables and it has the advantage of not requiring the knowledge of how variables are distributed. However, it should be applied only when variables are linearly related to each other.

A.2. Coherence

Coherence (magnitude squared coherence or coherence spectrum) measures the linear correlation among the two spectra[12]. To calculate the coherence spectrum, data must be in the frequency domain. In order to do so, time series are usually divided into *S* sections of equal size. The Fast Fourier Transform algorithm is then computed over the sections to get the

estimate of each section’s spectrum (periodogram). Then, the spectra of the sections is averaged to get the estimation of the whole data’s spectrum (Welch’s method). Finally, Coherence is a normalization of this estimate by the individual autospectral density functions [12]:

$$SC = \frac{|\langle Sp_{xy}^2 \rangle|}{|\langle Sp_{xx} \rangle| |\langle Sp_{yy} \rangle|} \quad (14)$$

where Sp_{xy} is the Cross Power Spectral Density (CPSD) of both signals, Sp_{xx} and Sp_{yy} are the Power Spectral Density (PSD) of the segmented signals X and Y taken individually, and $\langle \cdot \rangle$ is the average over the S segments. In the case of the data sets obtained with the nonlinear electronic Lorenz systems, frequencies higher than $f_{cut} = 7.5K$ Hz have been disregarded for the computation of SC , since the power spectra of the electronic circuits are completely flat above this frequency. One of the drawbacks of Coherence is that it doesn’t discern the effects of amplitude and phase in the relationships measured between two signals, which makes its interpretation unclear [23, 4].

A.3. Phase Locking Value

Phase Locking Value was first introduced by Lachaux et al. [23] as a new method to measure synchrony among neural populations. It has, at least, two major advantages over the classical coherence measure: it doesn’t require data to be stationary, a condition that can rarely be validated; and has a relatively easy interpretation (in terms of phase coupling). However, the methods used to extract instantaneous phase, a step needed to calculate PLV rely on stationarity, so indirectly PLV can be affected by this condition [24]. To obtain the PLV , the signal has to be decomposed to it’s instantaneous phases and amplitudes. To achieve this, there are several methods, such as Morlet wavelet convolution or Hilbert transform [12, 24]. In this work we will utilize the latter. Finally, PLV is obtained averaging over time t :

$$PLV = \frac{1}{N} \left| \sum_{n=1}^N \exp(i\theta(t, n)) \right| \quad (15)$$

where $\theta(t, n)$ is the (instantaneous) phase difference $\phi_x - \phi_y$, the phases to be compared from the signals X and Y . Comparisons are carried out pairwise (bivariate).

A.4. Mutual Information

Mutual Information is a measure of shared information between any components of a system, between systems, or any other parameter whose value's probability can be estimated. It is based on Shannon's notion of entropy, which, in a general sense, tries to quantify the amount of information contained in a random variable by means of its estimated probability distribution. Mutual information measures the amount of information *shared* between two random variables by means of its joint distribution, or conversely, the amount of information we can obtain from one random variable observing another. This is analogue to measuring the dependence between two random variables [25]. Let X and Y be two random variables with $\{x_1, x_2, \dots, x_n\}$ and $\{y_1, y_2, \dots, y_n\}$, n possible values with probabilities $p(x)$ and $p(y)$. The *MI* of X relative to Y can be written as:

$$MI(X \cap Y) = \sum_{x \in X, y \in Y} p(x \cap y) \log_2 \frac{p(x \cap y)}{p(x)p(y)} \quad (16)$$

$$MI(X \cap Y) = H(X) - H(X|Y) \quad (17)$$

where $p(x \cap y)$ is the probability that X has a value of x *while* Y has a value of y , $H(X)$ is the entropy of X and $H(X|Y)$ is the conditional entropy of X and Y . One of the major advantages of *MI* is that it captures linear and non-linear relationships among variables. One disadvantage is that it does not explicitly tell the shape of that distribution [24]. To get the mutual information between two random variables, we first need to estimate their probability density distribution [25, 24, 26]. Equation 16 compares joint probabilities against marginal ones. When two values are independent, the product of their marginal probabilities should equal their joint probability. When not, we can state that there is a relationship among them (not necessarily linear), because the probability of finding those values together is greater than the probability of finding them by chance. Thus, somehow, those time series are coupled, although we don't know the way it occurs.

Appendix B: Electronic version of the Lorenz system

The equations of the master and slave electronic Lorenz systems are:

$$V\dot{x}_1 = \frac{1}{R_1 C} \left(\frac{R_1}{R_2} V_{y_1} - \frac{R_4}{R_3} V_{x_1} + \frac{R_4}{R_3} V_{\xi_1} \right) \quad (18)$$

$$V\dot{y}_1 = \frac{1}{R_5 C} \left(\frac{R_5}{R_6} V_{x_1} - \frac{R_5}{R_7} V_{x_1} V_{z_1} \right) \quad (19)$$

$$V\dot{z}_1 = \frac{1}{R_8 C} \left(\frac{R_8}{R_9} V_{x_1} V_{y_1} - \frac{R_{11}}{R_{10}} V_{z_1} \right) \quad (20)$$

$$V\dot{x}_2 = \frac{1}{R_{12} C} \left(\frac{R_{12}}{R_{13}} V_{y_2} - \frac{R_{15}}{R_{14}} V_{x_2} + \frac{R_{12}}{R_{29}} V_{\xi_2} + \frac{R_{12}}{R_{30}} V_{\sin x} \right) \quad (21)$$

$$V\dot{y}_2 = \frac{1}{R_{16} C} \left(\frac{R_{17}}{R_{16}} V_{x_2} - \frac{R_{17}}{R_{20}} V_{x_2} V_{z_2} \right) \quad (22)$$

$$V\dot{z}_2 = \frac{1}{R_{19} C} \left(\frac{R_{19}}{R_{20}} V_{x_2} V_{y_2} - \frac{R_{22}}{R_{21}} V_{z_2} \right) \quad (23)$$

where $V_{x_{1,2}}$, $V_{y_{1,2}}$ and $V_{z_{1,2}}$ are the voltage variables of the master (sub-index 1) and slave (sub-index 2) Lorenz systems, $V_{in} = V_{x_1} - V_{x_2}$ is the coupling signal injected into the slave system in a diffusive way, $\kappa = \frac{R_{dp}}{C_5 R_{30}}$ is the coupling strength and $0 \leq R_{dp} \leq 1$ is the percentage of coupling controlled by the digital potentiometer. In the experiments where external noise is considered (see Appendix C), the amplitude of V_{ξ_1} and V_{ξ_2} are set to 0.5 V and zero otherwise.

Table 1 contains the parameters of the resistances and capacitances used in the experiments.

$R_1, R_{12} = 100K\Omega$	$R_2, R_{13} = 100K\Omega$	$R_3, R_{14} = 10K\Omega$
$R_4, R_{15} = 10K\Omega$	$R_5, R_{16} = 1M\Omega$	$R_6, R_{17} = 35.7K\Omega$
$R_7, R_{18} = 20K\Omega$	$R_8, R_{19} = 375K\Omega$	$R_9, R_{20} = 20K\Omega$
$R_{10}, R_{21} = 10K\Omega$	$R_{11}, R_{22} = 10K\Omega$	$R_{23} = 10K\Omega$
$R_{24} = 10K\Omega$	$R_{25} = 10K\Omega$	$R_{26} = 10K\Omega$
$R_{27} = 10K\Omega[0-1]$	$R_{28} = 100K\Omega$	$R_{29} = 100K\Omega$
$R_{30} = 100K\Omega$	$C_{1-6} = 1nF$	$V_+ = 15V, V_- = -15V$

Table 1: Parameters of the electronic components used for the construction of the Lorenz oscillators and the coupled circuit.

Appendix C: Robustness of OS in the presence of external noise

Figures 8-9 are equivalent to Figs. 3-4 but in the presence of external noise. In this case, we have introduced two noises ξ_1 and ξ_2 perturbing the x_1 and x_2 variables of the master and slave Lorenz systems as explained in Appendix B. Comparing Fig. 8 and Fig. 3 we can observe that all synchronization metrics have reduced their values in the presence of external noise, however, the behaviour remains qualitatively similar to the one reported in Fig. 3. Again, the case $D = 3$ is the one suffering the most from the presence of noisy signals (Fig. 8D). When comparing OS with the rest of synchronization metrics (Fig. 9), we can also observe a reduction of the correlations respect to the case without external noise. Again, r and PLV are the metrics showing higher correlation with OS , having a linear correlation for $D = 500$ and $D = 1000$. This correlation is impaired for $D = 3$, since it corresponds to the ordinal vector length that is more affected by noise. On the other hand, the nonlinear correlations with MI and SC remain quite similar as in the case of the absence of external noise.

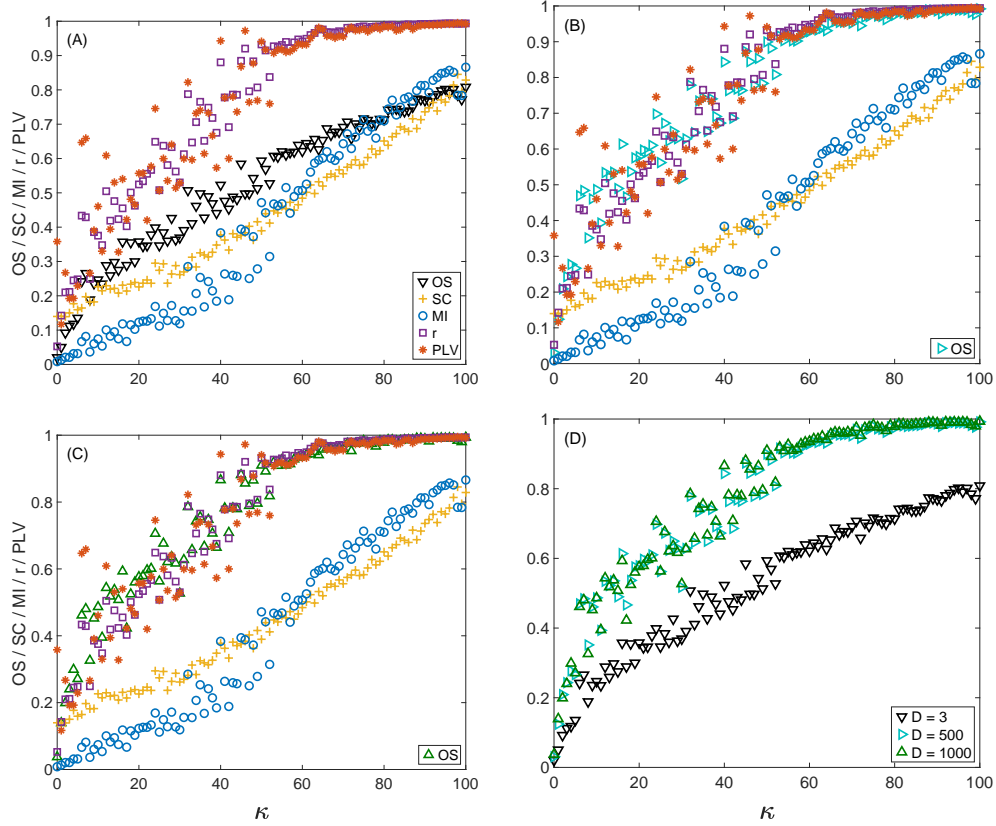


Figure 8: Synchronization against coupling strength κ , as measured with mutual information MI (light blue), spectral coherence SC (yellow), phase locking value PLV (red) Pearson correlation r (purple) and ordinal synchronization OS (black) for $D = 3$ (A), $D = 500$ (B) and $D = 1000$ (C). For comparison purposes, plot D shows OS against coupling strength for the different vector lengths, $D = 3$ (black), $D = 500$ (turquoise) and $D = 1000$ (green).

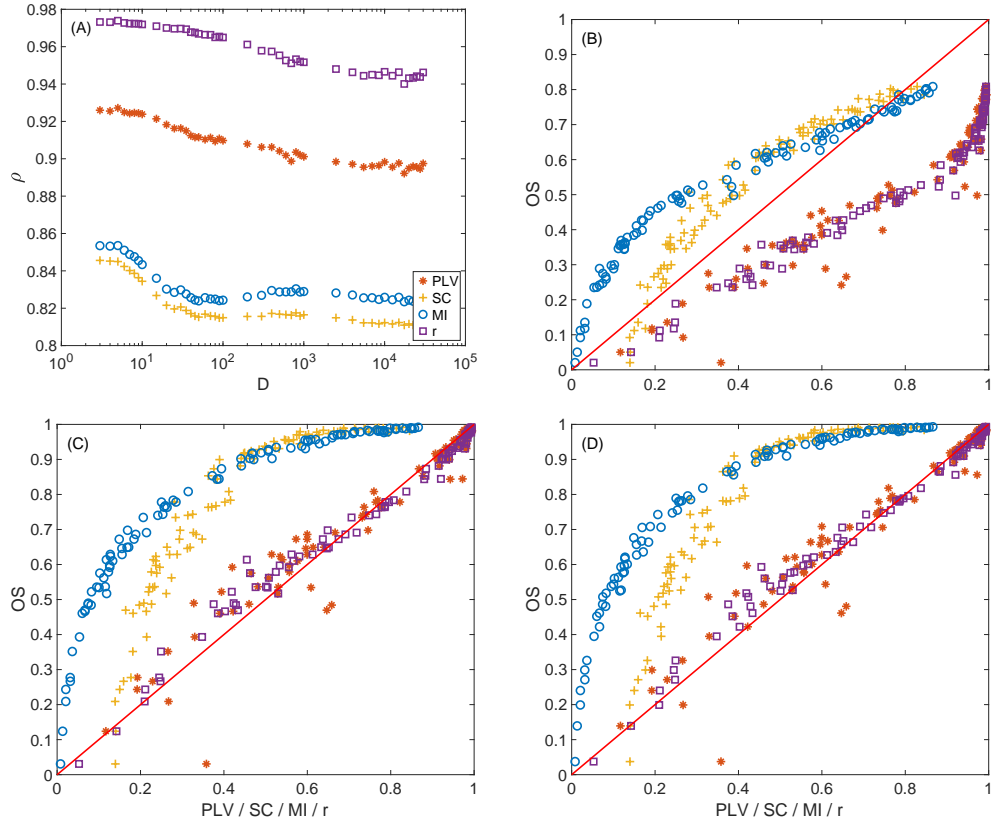


Figure 9: Panel A shows the average correlation between each synchronization measure and OS depending on the vector length (D) used to compute OS. Panels B-D show the correlation between OS and all other synchronization measures varying the coupling strength (from 0 to 100), for $D = 3$ (B), $D = 500$ (C) and $D = 1000$ (D). Synchronization measures are Mutual information (MI; blue), Pearson correlation coefficient (r ; purple), spectral coherence (SC; yellow) and phase locking value (PLV; red). The red line corresponds to $y = x$.

References

References

- [1] C. Huygens, in *oeuvres completes de christian huygens*, edited by M. Nijhoff (Societe Hollandaise des Sciences, The Hague, The Netherlands). 5 (1893) 246.
- [2] Z. Néda, E. Ravasz, Y. Brechet, T. Vicsek, A.-L. Barabási, Self-organizing processes: The sound of many hands clapping, *Nature* 403 (2000) 849–850.
- [3] R. Schmidt, C. Carello, M. T. Turvey, Phase transitions and critical fluctuations in the visual coordination of rhythmic movements between people, *J. Exp. Psychol. Hum. Percept. Perform.* 16(2) (1990) 227–247.
- [4] F. Varela, J. Lachaux, E. Rodriguez, J. Martinerie, The brainweb: phase synchronization and large-scale integration, *Nat. Rev. Neurosci.* 2 (2001) 229–239.
- [5] N. Agladze, O. Halaidych, V. Tsvelaya, T. Bruegmann, C. Kilgus, P. Sasse, K. Agladze, Synchronization of excitable cardiac cultures of different origin, *Biomater. Sci.* 5 (2017) 1777.
- [6] K. Romer, Time synchronization in ad hoc networks, in: *Proceedings of ACM Symposium on Mobile Ad Hoc Networking and Computing (MobiHoc)* (2001) 173–182.
- [7] B. Wang, H. Suzuki, K. Aihara, Enhancing synchronization stability in a multi-area power grid, *Sci. Rep.* 6 (2016) 26596.
- [8] A. Arenas, A. Díaz-Guilera, J. Kurths, Y. Moreno, C. Zhou, Synchronization in complex networks, *Phys. Rep.* 469 (2008) 93–153.
- [9] S. Boccaletti, V. Latora, Y. Moreno, M. Chavez, D. U. Hwang, Complex networks: Structure and dynamics, *Phys. Rep.* 424 (2006) 175–308.
- [10] E. Mones, N. Araújo, T. Vicsek, H. Herrmann, Shock waves on complex networks, *Sci. Rep.* 4 (2014) 4949.
- [11] C. Rech, R. Perret, Adding dynamics to the Human Connectome Project with MEG, *Int. J. Syst. Sci.* 21 (1990) 1881.

- [12] E. Pereda, R. Q. Quiroga, J. Bhattacharya, Nonlinear multivariate analysis of neurophysiological signals, *Progress in Neurobiology* 77 (2005) 1–37.
- [13] A. Bahraminasab, F. Ghasemi, A. Stefanovska, P. McClintock, H. Kantz, Direction of coupling from phases of interacting oscillators: A permutation information approach, *Phys. Rev. Lett.* 100 (2008) 084101.
- [14] M. Paluš, A. Stefanovska, Direction of coupling from phases of interacting oscillators: An information-theoretic approach, *Phys. Rev. E* 67 (2003) 055201.
- [15] Z. Li, G. Ouyang, D. Li, X. Li, Characterization of the causality between spike trains with permutation conditional mutual information, *Phys. Rev. E* 84 (2011) 021929.
- [16] E. Izhikevich, Simple model of spiking neurons, *IEEE Trans. Neural Netw.* 14 (2003) 1569.
- [17] R. Rosário, P. Cardoso, M. Muñoz, P. Montoya, J. Miranda, Motif-synchronization: A new method for analysis of dynamic brain networks with eeg, *Physica A* 439 (2015) 7–19.
- [18] E. Olofsen, J. Sleight, A. Dahan, Permutation entropy of the electroencephalogram: a measure of anaesthetic drug effect, *Br. J. Anaesth.* 101 (2008) 810–821.
- [19] C. Bandt, B. Pompe, Permutation entropy: a natural complexity measure for time series., *Phys. Rev. Lett.* 88 (2002) 174102.
- [20] E. Lorenz, Deterministic nonperiodic flow, *J. Atmos. Sci.* 20 (1963) 130–141.
- [21] <http://zone.ni.com/reference/>, National instruments, Noise (2018).
- [22] L. Larson-Prior, R. Oostenveld, S. Della Penna, G. Michalar-eas, F. Prior, A. Babajani-Feremi, J.-M. Schoffelen, L. Marzetti, F. de Pasquale, F. Di Pompeo, J. Stout, M. Woolrich, Q. Luo, R. Bucholz, P. Fries, V. Pizzella, G. Romani, M. Corbetta, A. Snyder, Adding dynamics to the Human Connectome Project with MEG, *NeuroImage* 80 (2013) 190–201.

- [23] J. P. Lachaux, E. Rodriguez, J. Martinerie, F. J. Varela, Measuring Phase Synchrony in Brain Signals, *Human Brain Mapping* 8 (1999) 194–208.
- [24] M. X. Cohen, *Analyzing Neural Time Series Data: Theory and Practice*, MIT Press, Cambridge, Massachusetts, 2014.
- [25] N. Veyrat-Charvillon, F.-X. Standaert, Mutual Information Analysis: How, When and Why?, *Cryptographic Hardware and Embedded Systems-CHES 2009. Lecture Notes in Computer Science (LNCS) 5747* (2009) 429–443.
- [26] B. Gierlichs, L. Batina, P. Tuyls, B. Preneel, Mutual Information Analysis A Generic Side-Channel Distinguisher, *Cryptographic Hardware and Embedded Systems-CHES 2008. Lecture Notes in Computer Science 5154* (2008) 426–442.